Biophysical Journal

Article



Phonon-assisted electron-proton transfer in [FeFe] hydrogenases: Topological role of clusters

Yann Chalopin, 1,* Stephen P. Cramer, 2 and Simon Arragain 3

1 Laboratoire d'Energétique Macroscopique et Moléculaire, Combustion (EM2C), CNRS/CentraleSupélec, University of Paris-Saclay, Gif-sur-Yvette, France; ²SETI Institute, Mountain View, California; and ³IFP Energies Nouvelles, Rueil-Malmaison, France

ABSTRACT [FeFe] hydrogenases are enzymes that have acquired a unique capacity to synthesize or consume molecular hydrogen (H₂). This function relies on a complex catalytic mechanism involving the active site and two distinct electron and proton transfer networks working in concert. By an analysis based on terahertz vibrations of [FeFe] hydrogenase structure, we are able to predict and identify the existence of rate-promoting vibrations at the catalytic site and the coupling with functional residues involved in reported electron and proton transfer networks. Our findings suggest that the positioning of the cluster is influenced by the response of the scaffold to thermal fluctuations, which in turn drives the formation of networks for electron transfer through phonon-assisted mechanisms. Thus, we address the problem of linking the molecular structure to the catalytic function through picosecond dynamics, while raising the functional gain brought by the cofactors or clusters, using the concept of foldencoded localized vibrations.

SIGNIFICANCE [FeFe] hydrogenases are enzymes that efficiently produce or consume molecular H₂ through the coordination of two separate electron and proton transfer networks during the catalytic process. Our research sheds light on a physical mechanism behind their biochemical activity by revealing that enzymes have adapted to react to thermal fluctuations via the vibrations of their molecular scaffold. The short-scale dynamics inherent in the folding of proteins offers a logical justification for the emergence of intricate biochemical functions observed in enzymes and proteins more broadly.

INTRODUCTION

Earth is experiencing adverse climate change caused by the unrelenting human-caused emission of CO2 into the atmosphere, which mainly originates from the combustion of fossil fuels (1). As one response for a much-needed paradigm shift, molecular hydrogen, H₂, has been touted as an ideal carbon-free energy vehicle (2-4). Adoption of H₂ could initiate a sustainable "hydrogen economy" without CO2 emissions, thus moderating the current trajectory of climate change (4-7). In this paper, we propose to better understand how Nature has solved the problem of producing and consuming H₂ in enzymes known as hydrogenases. [FeFe] hydrogenases are the fastest enzymes for reducing protons to H₂, which they accomplish at speeds rivaling the best Pt catalysts (2-4,6-11). One of the best studied of these enzymes is the [FeFe] hydrogenase from Clostridium pasteur-

Submitted November 1, 2022, and accepted for publication March 16, 2023.

*Correspondence: yann.chalopin@cnrs.fr

Editor: Diego Ferreiro.

https://doi.org/10.1016/j.bpj.2023.03.027

© 2023 Biophysical Society.

This is an open access article under the CC BY-NC-ND license (http:// creativecommons.org/licenses/by-nc-nd/4.0/).

ianum (CpI) (5). The enzyme's active site, known as the "H-cluster," is situated within a hydrophobic cavity located at the center of its most globular structural part. (Fig. 1 A). The H-cluster consists of a $[2Fe]_H$ subcluster linked to a [4Fe-4S] cluster by a cysteine thiolate (Fig. S1). Electrons and protons are conveyed to the H-cluster along two distinct transfer paths. The pathway for electrons involves three [4Fe-4S] clusters as well as a [2Fe-2S] cluster (Fig. 1 A). The pathway for protons has also been identified, and the importance of the conserved amino acids along this path has been confirmed by systematic mutation to alanines (12). Despite the many studies regarding the catalytic mechanisms of [FeFe] hydrogenases, very few have emphasized the importance of the terahertz (THz) dynamics, i.e., the thermal vibrations (13,14). Some studies have certainly evoked elements going in this direction by reporting stabilization effects, i.e., local increase of the energy associated with the cohesion of a structure. It is essential to recognize that proteins are dynamic structures that continuously undergo thermal fluctuations. Although we refer to these systems as "thermally evolved," descriptions of their Chalopin et al.

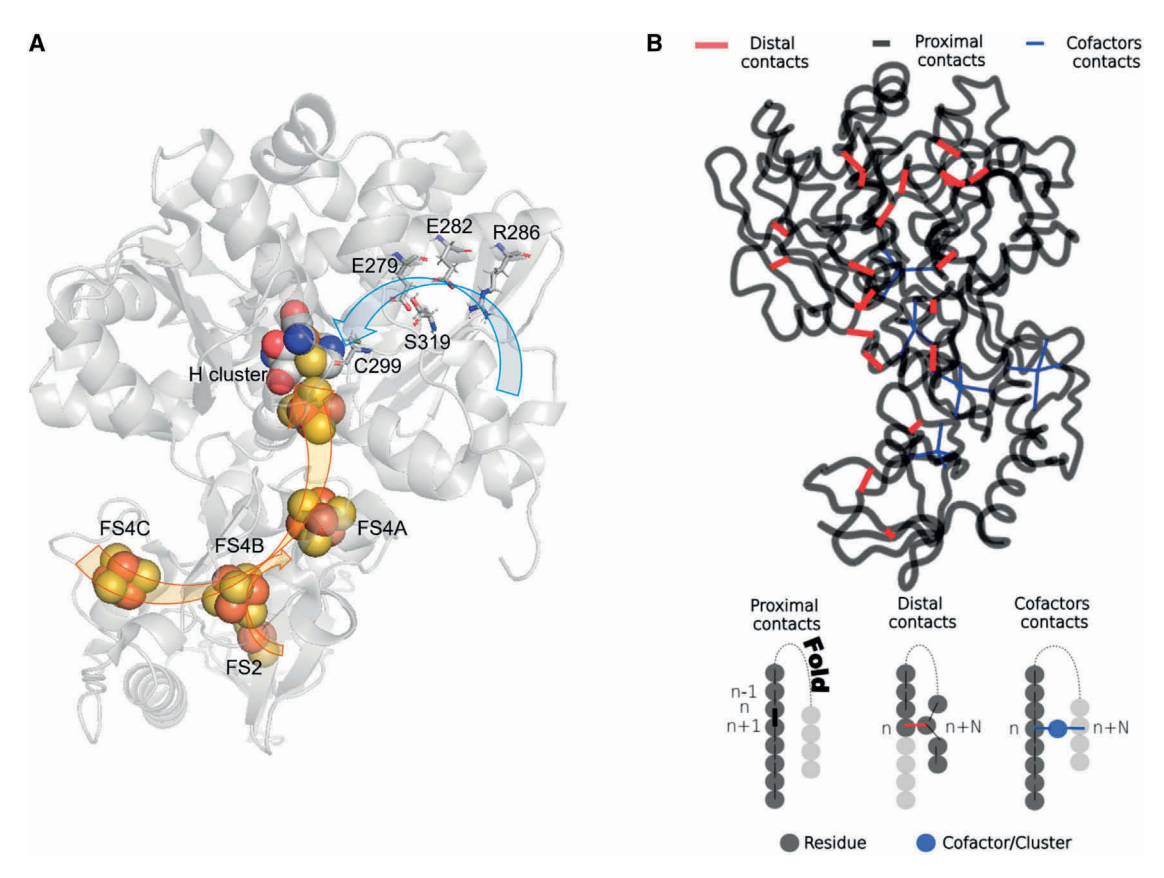


FIGURE 1 Structure and topology. (A) [FeFe] hydrogenase (CpI) with the H-cluster and the four FeS clusters (PDB: 4xdc) as well as the residues involved in the proton transfer network (blue arrow). The putative electrons pathways appear under the red arrows. (B) Topologically, folded protein corresponds to the perturbation of a regular AA chain made of proximal contacts every 3.8 A into a 3D structures that will form new contacts: distal contacts with other residues or cofactor contacts with the mean of ligands interactions. To see this figure in color, go online.

functioning as static entities only provide a limited understanding of their behavior.

By analyzing the enzyme's vibrational properties on fast timescales (picoseconds), we can gain insight into the physical characteristics of these transfer paths. They also help us perceive the interplay between the structure and the function—moving charges via two transfer networks proceeding in concert. In particular, we formulate a theory to understand how a given molecular structure, under the effect of thermal energy fluctuations of the environment, produces a partition of local, coordinated, and coupled motions allowing the selection of a molecular function (in this case, catalysis, and the consecutive transfer of charges upstream and downstream of the cavity). To this purpose, we pair the concepts of "rate promoting vibrations" (RPVs) (13-15) with that of "fold encoded localized vibrations" developed in a previous study (16,17). RPVs correspond to compressions that optimize the donor-acceptor separation, thereby increasing the transfer probability via vibrationally assisted coupling in the THz range. The role of the fluctuations provided by RPVs in the active site region was established quantum mechanically in the 1990s (18), but also using kinetic isotope effects experiments (19). Later, Schwartz and co-workers provided a classical description of RPVs through transition path sampling (20). Similarly, the theory introducing the concept of fold encoded localized vibrations (16,21) describes RPVs as a classical wave-like phenomenon driven by an effectivestructural encoded—confinement potential. The role of RPVs in enzymes was also highlighted for the tunneling reaction coordinate in lactate dehydrogenase (22). Alternatively, promoting vibration coupling directly to the reaction coordinate in enzyme-catalyzed proton transfer reactions has been observed through a kinetic isotope effect (23). Other important works involving similar experiments made no reference to fast vibrations in describing their results theoretically (24). We show that it is possible to associate with the molecular structure of [FeFe] hydrogenase (PDB: 4xdc) (25) a pattern of localized vibrations that provides a physical rationale for understanding how networks of charge transfer emerge in a protein structure (and by extension to its sequence). From the protein topology and the positions of theses clusters, we describe the emergence of a dynamic network that gives rise to vibrationally induced active conformations. Our analysis of a regular subnetwork has revealed the presence of complex dynamics that could have functional implications. These dynamics occur on characteristic timescales of the order of

picoseconds and involve atomic fluctuations ranging from ~ 0.5 to ~ 1.2 A, as illustrated in Fig. 4 C.

Cpl [FeFe] hydrogenase structural description

There are two main types of iron-sulfur (FeS) clusters found in hydrogenases: FE4S and FE2S. The FE4S cluster is a cuboidal structure consisting of four iron atoms coordinated by four sulfur atoms. In contrast, the FE2S cluster is a tetrahedral structure consisting of two iron atoms coordinated by two sulfur atoms. The CpI enzyme contains several FeS clusters. Three of them are [4Fe-4S] clusters (FS4CA, SF4B, and SF4C) allowing electron transfer coming from the ferredoxin toward the H-cluster (Fig. 1 A).

The ligands associated with the first cluster consist of three cysteines, C98, C101, and C107, and one histidine, H94. The second cluster interacts with cysteines C147, C150, C153, and C200. The third cluster is associated with four cysteines residues C157, C190, C193, and C196. In addition, a [2Fe-2S] cluster (FS2) is bound by ligands C34, C46, C49, and C62. Finally, the H-cluster forms the active site of the CpI. It corresponds to a [4Fe- $4S_H$ cluster with cysteine ligands C300, C355, C499, and C503 (Fig. S2). In addition, the cysteine C503 bridges to the $[2Fe]_H$ subcluster composed of two irons connected by a 2-azapropane-1,3-dithiolate (ADT) bridge (Fig. S2). Irons of this subcluster are ligated by one CO and one CN molecule plus a bridging CO between the two irons (26,27) (Fig. S3). A proton transfer chain has also been described in CpI. This allows an optimal proton transfer from external solvent water to the bridging amine present in the subcluster. Pathway 1 is composed of residues R286, E282, S319, and E279, a water molecule, and C299 (5) (Fig. S3). The H-cluster is present in a cavity where additional residues are important for the enzyme activity (28). As an example, CpI M353 variants, which change the interaction with the bridging CO (Figs. S1 and S2), offer a different configuration that might facilitate capture of H₂ (29) (Fig. S2). The H-cluster binds hydrogen species in an apical position or Fe-Fe bridging position (30). Thus, CpI M353 variants might constitute a vibrational hotspot that could impact the capture of an H₂-bound intermediate. M497 is also relevant because this methionine is at the opposite side of the protonated amine of the ADT bridge (3.7 A way from ADT amine) (see Fig S2). In addition, residues K358, P324 and Q325 have close interactions with the distal CN of the $[2Fe]_H$ subcluster. Other residues are also important (S323, I268, A230, P231, S232, P354, F417, and V423) because they participate in the formation of a cavity with a characteristic length of approximately 4 A (see Fig. S2). This scale is—as exposed in the following analysis—fundamental for understanding the thermal and therefore dynamic properties of these enzymes. A 3D representation of these cavity residues is depicted in the supporting material (Fig. S2). In hydrogenases, electron transfer occurs mainly through the three [4Fe-4S] clusters presented above up to the H-cluster (31,32). This electron transfer is coupled with the proton transfer (31) in a so-called proton-coupled electron transfer that occurs with a low activation barrier (24,33).

MATERIALS AND METHODS

The localization of fast vibrations

Enzymes are highly dynamic structures exhibiting thermally activated motions over timescales ranging from slow conformational changes (milliseconds) to the barrier crossing at the chemical step (femtoseconds). Theoretical studies that emphasize dynamic effects to explain enzyme function often rely on molecular dynamics (MD) simulations and normal mode analysis. It should be noted that the latter approach often focuses on the lowest energy modes, i.e., the slowest, but corresponding to the largest displacement amplitudes, involving a small fraction of large molecular domains. Such motions represent only a tiny fraction (< 1% as the total number of modes corresponds to ~ 3 times the number of amino-acids [AA]) of the total vibrational energy carried by the molecular scaffold. However, some authors have suggested that thermal vibrations on a picosecond timescale are essential for an enzyme to function (13,14,16,17,34). Nevertheless, understanding dynamic determinants on this timescale requires significant computational resources and the analysis of trajectories obtained by simulations remains extremely tedious. In order to-but not only toovercome these limitations, we have developed a theory that captures in a simple representation the full dynamic pattern of enzymes to visualize and detect their functional properties over timescales ranging from nanoseconds to picoseconds. This approach focuses on the phonon properties of the protein backbone (BB) and considers the coexistence of structural regularities associated with the polypeptide chain and the disrupted symmetry introduced by its folding. This structural competition between order and disorder produces the entanglement between a propagation phenomenon (thermal waves) and interference patterns within the structure, which ultimately create thermal hotspots. These "spots" are not at a higher temperature than the other regions (which would violate thermodynamics); rather, there is a higher density of THz phonons concentrated in these regions. As explained below, the latter have been selected throughout evolution to enable a molecular function such as the oxidation of H2 or the reduction of protons with energy-conserving transfer chain reactions. A previous study (16) established that such thermal spots correspond to small domains (~ 10 residues). It turns out that the majority of active sites in enzymes are located in close proximity to such domains (16). A thorough analysis of these thermal hotspots allows the pairing of a biophysical function with the concept of RPVs, which is enabling the modulation of the reaction barrier at the active sites by means of structure-dependent thermally activated modes. We demonstrate here, but in a rather different way, that these rapid localized phenomena produce local thermal fluctuations that are crucial for the understanding of the functioning of hydrogenases and the regulation of their chemistry. Before that, several definitions are introduced.

Thermal contacts in a complex folded structure

Understanding the phenomenon of thermal localization of phonons in enzymes requires the introduction of the characteristic lengthscale of 3.8A corresponding to the $C\alpha$ periodicity within the polypeptide chain. This length defines a pseudo period (or the Brillouin zone) allowing the existence of phonon modes in the AA chains corresponding to the enzymes' sequences. Later, we use it to define a map of thermal contacts within the folded structure. As shown later in this work, this topological consideration Please cite this article in press as: Chalopin et al., Phonon-assisted electron-proton transfer in [FeFe] hydrogenases: Topological role of clusters, Biophysical Journal (2023), https://doi.org/10.1016/j.bpj.2023.03.027

Chalopin et al.

can be extended to ligands and cofactors as well: an enzyme is a folded lattice in which cofactors bridge the topological gap in a 3D network (PDB: 4xdc).

Fig. 1 B illustrates a network formed by $C\alpha$ and cofactor atoms separated by 3.8 ± 0.5 A; 0.5 A is the error margin in the measurement of the distance between atoms, which can vary due to thermal fluctuations within the stiffer regions of the molecule. This topological representation of the enzyme complex accounts for three types of edge: 1) the BB $C\alpha$ interdistance along the sequence (gray), 2) the interdistances with $C\alpha$ not consecutive along the sequence (red), and 3) a 3.8 ± 0.5 A interdistance with $C\alpha$ and H-clusters and FeS-clusters (blue). Interestingly, this reveals that particular residues that are distal along the sequence 2) are more favorably coupled by the folding. Furthermore, additional couplings between the residues appear to be operated by the cofactors. These topological properties serve as a basis for further dynamical analysis unveiling the functional role of localization thermal spots.

The localization landscape of vibrations

As shown previously, the pattern of localized vibrations is visualizable in a quite convenient way using a mathematical tool termed localization land-scape. In the supporting material, we have included a brief tutorial on how to calculate this quantity using a simple example that is analytically solvable. We recall here the basic steps that lead to an efficient computation of this quantity, and which will be referred to continuously in the rest of this paper. In harmonic regime, the dynamic equation of the interacting AA in a folded chain is written

$$(C - \omega^2)\widetilde{X}_i = \left(C - \sum_{j=1}^N \alpha_{ij}\right)\widetilde{X}_i + \sum_{j=1}^N \alpha_{ij}(-1)^{|j-i|}\widetilde{X}_j,$$

(Equation 1)

where ω , X_i , α_{ij} , and C are, respectively, the vibration pulsation, the displacement amplitude of the residue i, and the mass weighted force constant accounting for the C_α masses $m_{C\alpha}$. In a matrix form involving the operator L_h , the dynamic equation writes

$$L_b \tilde{X} = (C - \omega^2) \tilde{X},$$
 (Equation 2)

where the quantity u_h identifies the ability of each residue to localize thermal energy. It is obtained by the resolution of the linear system

$$L_h u_h = (1).$$
 (Equation 3)

The precision of the calculation hinges on the reliability of interatomic potentials. In this work, a coarse-grained elastic model was employed to deduce the dynamic matrix of the system (L_h) , yielding outcomes on a par with those obtained via MD simulations. Nevertheless, the current elastic models' inadequacy in accounting for clusters or ligands poses a limit, and the inclusion of these interactions would certainly elevate the predictive accuracy of this approach.

RESULTS

The topological role of the clusters

This section aims at defining how the thermal hotspots are distributed around the active site as well as around the FeS clusters. We plotted the localization landscape computed using an elastic and molecular dynamic model (Fig. 2 A). We then compared how this landscape predicts the spatial confinement of vibration modes as a function of their frequencies (Fig. 2 B). Fig. 2 C presents the struc-

ture of the localized vibrations color coded along the sequence (chord plot) as well as in the 3D space (Fig. 2D).

To incorporate the concepts of contacts introduced previously, we associate thermal contacts (distal, cofactor, and proximal) to this structure and see how they possibly produce dynamic coupling between the enzyme thermal spots. The reasoning of this approach is to check whether thermal hotspot residues dynamically couple to the clusters to form a network of coupled residues that could match with charge transfer pathways. Therefore, we have first identified which thermal contacts between AAs are distant by $a = 3.8 \pm 0.4$ A but not consecutive on the sequence (distal contacts). To quantitatively estimate these couplings, the force constants were extracted from the dynamic matrix obtained by the MD simulation using the Amber force field for the proteins atoms and the TIP3P force field for the explicit water solvent (see supporting material for more details). The results of this calculation (Fig. S4) show at first glance that folding allows several residues to become dynamically coupled in the THz regime (16,17). Surprisingly, we notice that several thermal hotspots are connected through contacts. In particular, we see a small domain centered on residue R540 that couples with two other domains centered on residues F417 and I268, respectively. There is also significant coupling between domains centered on residues H500 and S232. Using MD, we checked that the displacement amplitude (see Fig. 4 C) of those residues is of the order of ~ 0.5 A at 300 K, as confirmed by the localization landscape from the formula $\langle X_i \rangle = \frac{1}{\sqrt{m_{C\alpha}}} \left(\frac{k_B T}{C - u_h^{i-1}} \right)$ (Fig. 4). Next, in a similar fashion, we have investigated whether the FeS clusters play a topological role allowing complementary couplings between other molecular domains. The polypeptide combined with the FeS clusters enables such effects (Fig. S4 B). The cysteine ligands that bind the [4Fe-4S] clusters are all associated with thermal hotspots. Indeed, these cofactors are inserted in cavities produced by the folded structure of AA. We found they play the role of enhancing the connectivity of a pre-established contacts network by inserting themselves in "gaps" of the regular lattice forming cofactor contacts. In an interesting way, these couplings involve even more thermal hotspots. We have looked at how they are distributed around the catalytic site to check if catalytic activity is subjected to fast vibrations (Fig. S4 C). We have considered the center of mass formed by the H-cluster atoms, and we looked at the distance between the H-cluster and the C_{α} forming the catalytic cavity. Not surprisingly, we found that the smallest H-cluster-AA distance is 3.8 ± 0.5 A. As shown in Fig. S4 C, this proximity concerns residues M229, A230, P231, S323, P324, F417, and M497. Thus, the H-cluster is at the center of a regular 3.8 ± 0.5 A network while a single residue (C503) keeps the H-cluster in the center of its

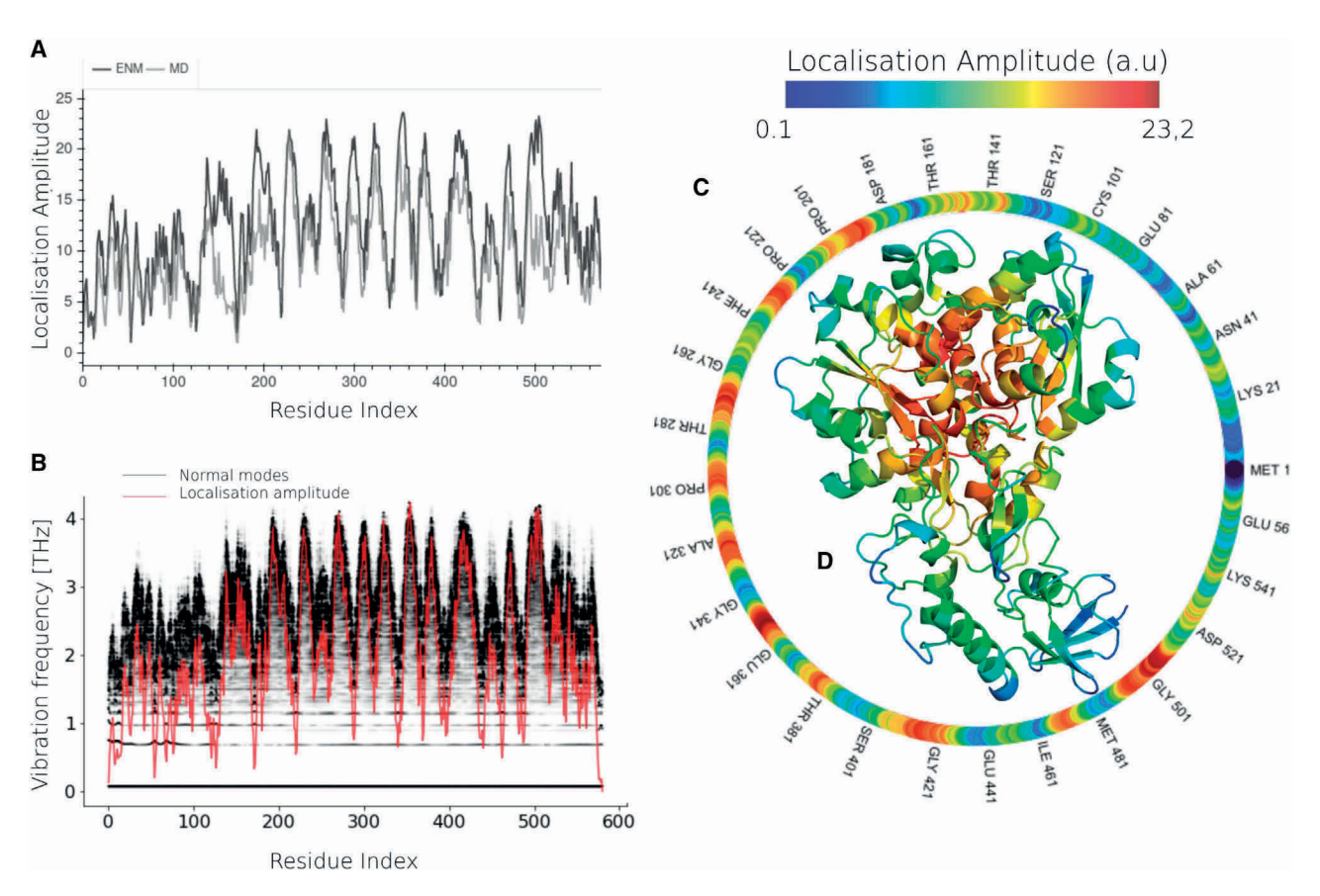


FIGURE 2 Localization landscape of the phonons. The localization landscape (LL) computed from MD simulations compared with that obtained with ANM-PfENM force field (A). Thermal hotspots are defined as compact domains of residues subjected to a structurally enhanced density of states of THz modes (B). The higher the localization amplitude (red), the faster the period of the corresponding phonon mode (B). The LL is plotted along the sequence as a chord plot (C), revealing about 10 hotspots. The LL allows detection of thermal hotspot residues (red) which form a particular 3D structure (D). To see this figure in color, go online.

pocket. It is worth reiterating that this pocket comprises four of the enzyme's primary hotspots, which necessitate the recruitment of nearly half of the total residues. The position of the H-cluster has also been compared with those of the FeS clusters. Here again, we find distances between the H-cluster atoms and the S atoms of the FS4A cluster ranging between 3.8 and 4.1 A; thus, the H-cluster and the FeS clusters belong to a regular network. Therefore, through the intermediacy of a FeS cluster, the H-cluster is dynamically coupled to its pocket cavity and also belongs to the network of coupled residues created by the FeS clusters.

DISCUSSION

We investigated the active site of [FeFe] hydrogenases and found that it is connected to multiple groups of residues characterized by THz thermal modes. The H-cluster, which plays a critical role in the enzyme's function, is located at the center of this cavity and is subjected to a significant population of fast phonon modes on the order of picoseconds, resulting in atomic displacement amplitudes of approximately 0.5 A. Here, we aim to demonstrate how the intricate network of coupled residues and clusters aligns with the proton and electron transfer pathways. We have summarized the full set of previously established thermal contacts in Fig. 3 A and overlaid them with experimentally identified residues involved in electron and proton transfer networks (EPTNs). Remarkably, we observed that all the residues essential to catalysis and EPTNs are located in thermal hotspots. To highlight the localized and compressive nature of the vibrational modes in the molecular BB, we have superimposed a calculation of the eigenmodes for the two highest-frequency modes onto a 3D representation of the localization landscape (Fig. 3 B). These eigenmodes were obtained by considering the dynamic matrix derived from the α_{ii} coefficients outlined in Eq. 1. The figure clearly shows how the cavity undergoes displacement patterns that tend to compress the residues within the pocket containing the H-clusters (C299, P324, M353, and M358). The modal structure appears to promote compression between residues along a different path involving also cluster FS4A. Given the vast number of eigenmodes associated with this enzymes (1719), it is challenging to gain a Chalopin et al.

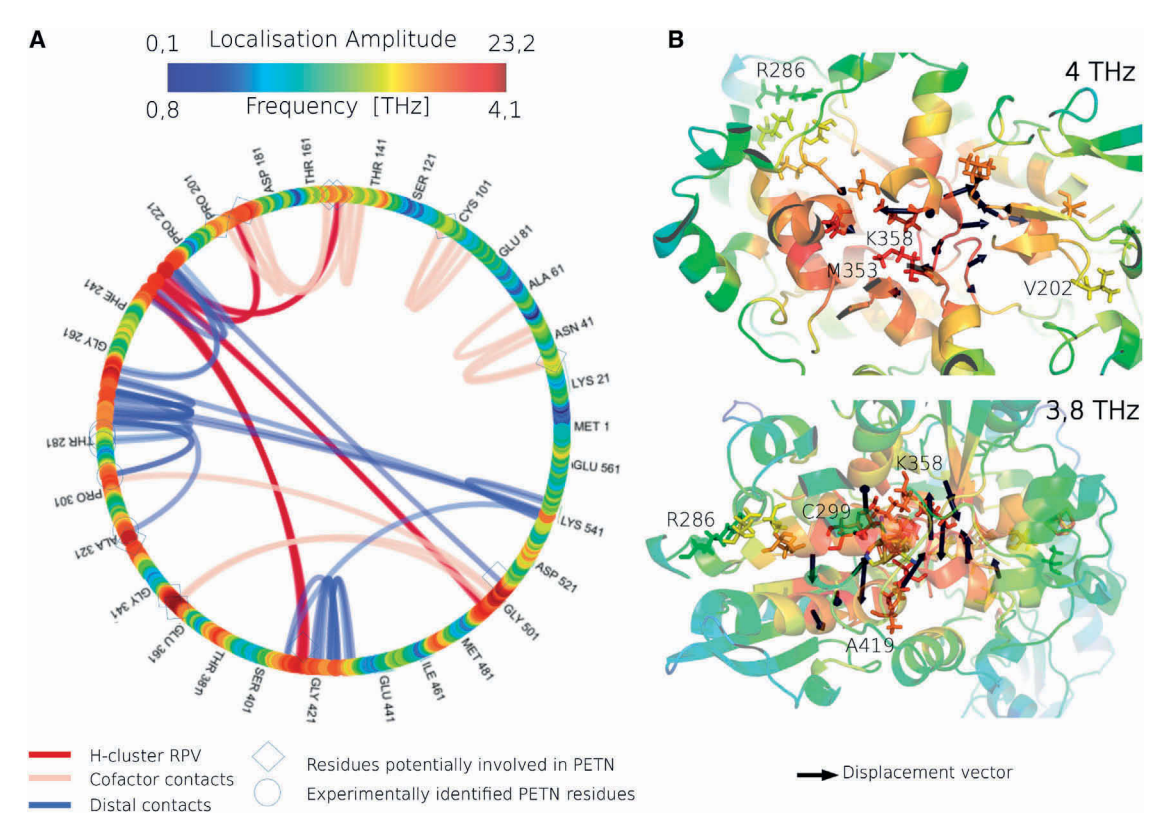


FIGURE 3 Vibrational hotspots and RPVs. Summary of the different contacts between the hotspots (A). The catalytic pocket forms a network of coupled residues with the H-cluster. Each FeS cluster exists in a cavity of compressive motions. (B) RPVs and corresponding ranked fastest frequencies. The locations of the RPVs match the catalytic residues. As can be observed, they correspond to localized compressive motions in the proximity of thermal hotspots. The correspondence between localization and the local vibration frequency v_i appearing in the legend is given by the relation $C - (2\pi v_i)^2 = 1/(C - u_h^i)$ (21). To see this figure in color, go online.

comprehensive understanding of the residues' dynamics, which is where the localization landscape becomes valuable as a visual representation.

Electron transfer pathways

Experimental investigation into the transfer of electrons in [FeFe] hydrogenases has been limited, as noted in previous studies (35,36). As of yet, there is no consensus regarding the exact mechanism and pathway of intermolecular electron transfer, despite two potential channels having been proposed for transferring electrons from ferredoxin. The first channel involves the three [4Fe-4S] clusters (FS4A, FS4B, and FS4C) and the H-cluster, while the second channel omits the FS4C cluster and instead incorporates the FS2 cluster. In this section, our objective is to examine whether the presence of RPVs in close proximity to the clusters can provide insight into identifying the specific residues that perform a functional role in the transfer process. As established previously, the H-cluster exhibits coordination with a pocket that encompasses hotspots associated with THz movements, which correspond to highly localized compressions measuring less than 0.5 A (as depicted in Fig. 3 A). Furthermore, we have found that each iron-sulfur cluster is connected to other thermal hotspots in the system, as all clusters exhibit interactions with each hotspot (thus, there is no hotspot not associated with a cluster). However, as one proceeds further away from the active site, i.e., as clusters become increasingly distant from the H-cluster, these hotspots exhibit associations with softer regions—that is, they correspond to slower localized modes with larger amplitudes. Consequently, the FS4B and FS4C clusters experience displacement fluctuations 2 to 3 times greater than those observed at the active site (see Fig. 4 A-C). It is worth noting that electron transfer to the active site of the enzyme has been shown to activate an important water channel (37), which facilitates the coordination of proton and electron transfer. This opening is triggered by the separation of a loop containing Gly418 and Ala419 from another loop containing Gly502 and Cys503 (as depicted in Figs. 3 A and 4 A). Again, this region corresponds to a thermal hotspot. We believe that fast localized modes (THz) in the active site region and its proximity correspond to RPVs that promote transfer phenomena by lowering energy barriers through thermally induced residue motions. However, as we move away from the active site and toward the solvent, local movement fluctuations inevitably become much greater, since the proximity of the solvent implies a

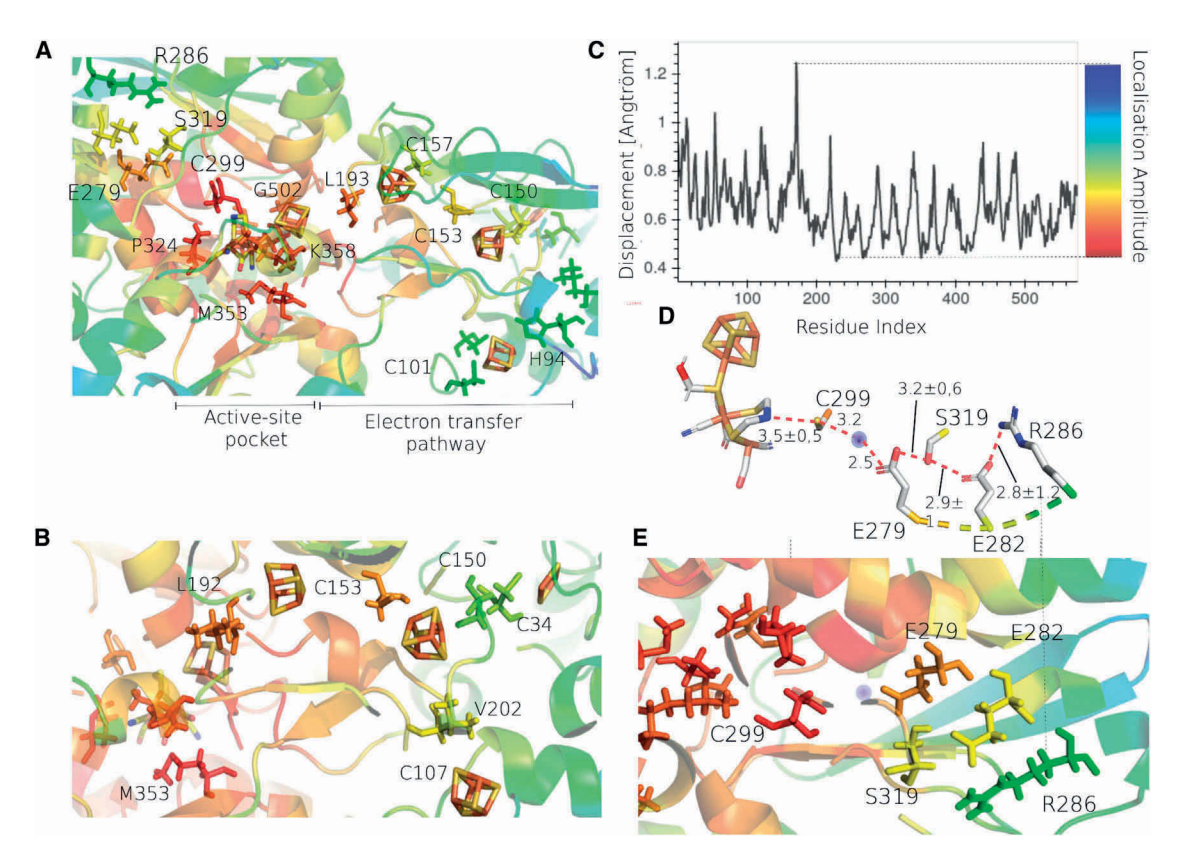


FIGURE 4 Electron and proton transfer pathways. The electron transfer pathway accounts for RPVs in the cavity (A) plus a network of clusters coordinated by hotspots (B). This description involves additional residues, which potentially mediate the transfer by modulating the tunneling barriers between the different FeS clusters. From our dynamical analysis, two pathways are possible (C). The proton transfer pathway involves a regular network of residues that undergoes picosecond thermal fluctuations (D). RPVs are found closed to the catalylic pocket (E), which is dynamically linked to a loop defining a stiffness gradient (R286, E282, E279). This gradient (E) allows the slower residues in contact with the solvent (R286) to efficiently couple to catalytic sites. To see this figure in color, go online.

reduction in cohesion energy. Since transfers between clusters occur through a diabatic transfer, it is necessary to strike a compromise between the stability required to keep the clusters stable at distances that do not fluctuate too much and can lead to another regime of transfers (adiabatic) while still maintaining thermal effects that modulate barriers. The five clusters integrate distances between neighboring clusters of approximately 8 and 12 A. The position fluctuations can bring the clusters closer by 1 A for the innermost clusters (FS4A-FS4B) to 2 A for the most distant clusters (FS4B-FS4C or FS2). Thus, thermal effects can lead to barrier reductions associated with widths reduced by about 10-15%. We are not able to quantify the impact of this modulation on the transfer process in this work. It is worth noting that Gauquelin et al. (35) have pointed out the importance of the loop containing two cysteines C34 and C45, associated with the binding to SF2, highlighting the importance of the dynamics of this loop-and notably its conformational rearrangement in the redox mechanism. Here, we show that this rearrangement occurs on timescales of the order of picoseconds. In their study (35), the same authors highlighted the importance of the FS2 cluster, which acts as a gateway for electrons. We were not able to demonstrate

sufficiently the importance of the transfer pathway involving this cluster compared with that involving the [4Fe-4S] clusters (FS4A, FS4B, and FS4C). However, our study reveals that the latter pathway involves compressions at higher frequencies, therefore faster but with lower amplitudes of fluctuations. The FS2 cluster is associated with movements that are approximately two times slower and therefore potential energy barrier compression amplitudes that are potentially two times larger (corresponding to a structurally less-stable region). We have reasons to believe that, if there is competition between these two transfer pathways, FS2 is probably more efficient at diabatically transferring electrons. The same authors, however, demonstrated that FS2 appears to be the main entry point for electrons, highlighting the ferridoxin's ability to preferentially bind in the vicinity of the FS2 cluster. We are unable to say here what results from the competition between barrier compression, chemical affinity, and modulation frequency, making it difficult to evaluate the predominance of one pathway or the other. Instead, we propose another transfer mechanism. To do this, we associated each pair of clusters, FS4A/FS4B, FS4B/FS4C, and FS4B/FS2, with an intermediate residue to complete a spatially regular residue Chalopin et al.

sequence of about 4 A. We identified residues C37, C150, C193, C153, and V202 (Fig. 4 B), noting that the cysteines also correspond to the cluster-binding sites. Thus, we have two regular networks of residues whose interdistances are modulated by thermal fluctuations. We conjecture that the RPVs, like the active sites, will allow electrons to transfer from one residue to another (by hopping) once the appropriate displacement fluctuation has reduced the energy barrier. In this case, the transfer is adiabatic. We hypothesize—without providing evidence here—that these transfer pathways, since they involve dynamically coordinated residues, should correspond to pathways with a predominant thermal dissipation. We believe that there is colocalization between electron transfer and thermal fluxes producing dissipation between residues. Thus, we see two perspectives: the first being experimental and involving the investigation of the role of residues mentioned above, while the second is theoretical and involves investigating whether there is colocalization between thermal and electron fluxes.

Proton transfer pathway

There is a consensus (31,37–39) on the network of residues involved in the transfer process (R286, E282, S319, E279, and C299), although the dynamic nature of proton transfer has been addressed experimentally, highlighting the importance of residues E141, E144, and R148 (40). Recently, it has been seen that CN- affects the proton transfer pathway (41), but this effect was not studied in this work. In what follows, we consider four transfer segments:

- the proton transfer from the ADT ligand of the H-cluster to the C299 residue
- from C299 to E279 + $(H_2 O)$
- proton transfer through residues E279-S319-E282
- E282-solvent

Regarding previous theoretical works, we agree with some observations made by Hong et al. (38) and Long et al. (39). These works are based on QM/MM calculations and consider thermal phonon modes associated with the protein structure. They observed that proton transfer times between donor and acceptor range between 0.7 and 3.1 ps, corresponding exactly to the periods of the localized BB vibrations mentioned throughout this article. They also reported displacement fluctuations in agreement with our prediction (Fig. 4 C). These lengthscales are an obvious manifestation of localized compression modes. In another work, Sode and Voth (37) highlighted the possible implication of a water channel in the proton transfer pathway. Unfortunately, our current model does not yet capture the dynamic effect of water molecules within the protein structures.

Although the centers of mass of those residues (R286, E282, S319, E279, and C299) are quite separated (± 6 A), they correspond to a sequence of donors and accep-

tors that form an H-bond network from the solvent to the H-cluster. From the PDB file (PDB: 4xdc), we extracted the distances between the donor and acceptor for H-bonds and complemented this topological property with how these distances fluctuate temporarily under the influence of vibrations produced by the thermal environment. These quantities were validated by MD simulation as well as by the calculation of the localization landscape following the procedure described in the caption of Fig. 2. In addition, we have accounted for the fact that, from the core to the surface of the protein in contact with the solvent, the rigidity decreases, thus allowing more amplitude oscillation. Again, this observation demonstrates that this H-bond network is sensitive to thermally induced displacement fluctuations, as it produces a channel of thermal contact of a maximum period of 3.9 A (an average extracted from Fig. 4 D), consistent with the theory underpinning localized phonons (Fig. 4, D and E). Hence, any structural perturbation that impedes the regularity of the H-bond lattice over distances greater that 3.8 ± 0.5 A would dramatically affect the proton transfer kinetics. This effect has indeed been observed experimentally by Happe and co-workers (31), who mutated the Glu to Asp, thus increasing the previous H-bond distance up to 6 A between R286 and E282. This had the effect of quenching the transfer channel and dramatically slowing down the transfer process by decoupling the residue in contact with the solvent from the RPV network. On the other hand, the local rigidity differs from the residues at the core to those in proximity with the solvent. Hence, the displacement amplitudes are much higher for residues R286 and E282 and occur at lower frequency (0.8 THz corresponding 26.7 cm⁻¹). Protons are transferred by hopping between the H-bonds of the residues and the water molecules forming the H-bond network with timescales ranging progressively from 0.25 to 1.25 ps. It is well established that this transfer of protons corresponds to a Grotthuss mechanism (42); that is, a lack of protons at the active site and along the chain tends to initiate the transfer mechanism by pumping or depletion up to the solvent. Once this process propagates, the formation and the subsequent breaking of H-bonds occurs along specific donor/acceptor paths. As with electrons, a new conjecture posits the possible colocalization of charge flow and thermal dissipation. Specifically, the optimization of distance modulation transfer between the donor/acceptor network that spans from the rigid active site to the pliant solvent implies the optimization of the heat flow from C299 to R286. Could this suggest that C299-R286 constitutes a predominant thermal dissipation channel from the active site to the surface?

Two mechanisms that occur in concert

In the case of the [FeFe] hydrogenase, proton transfer takes place over a considerable distance of more than 12 A. The long distance is counterbalanced by low free energy barrier

(maximum 5 kcal/mol) as reported by quantum calculations (32). However, we have shown that these barriers are modulated by particular atomic displacement patterns; that is, thermal hotspots that eventually enhance the tunneling transfer via coexisting and complementary mechanisms: THz modes and thus the associated picosecond local resonance stabilize the reactions by insulating the catalytic process from external mechanical perturbations (e.g., molecular collisions with solvent or external molecules) of large amplitudes. Moreover, hotspot residues involved in the proton transfer channel have a much higher density of vibrational states which results in a higher entropy. This means that, locally, a hotspot residue explores the space of molecular configurations much more efficiently (compared with residues in the valleys of the localization landscape) and they do so with characteristic time compatible with the timescale of the barrier crossing of the chemical reactions (a few femtoseconds). We have shown previously that the vibration amplitudes of the fastest and most localized modes (e.g., at the level of the active site) have a spatial extension of ± 0.5 to 1.2 A, implying an equivalent modulation of the interatomic distances (namely the H atoms). Under the action of these very localized fluctuations, the atoms of the different residues will move closer together, lowering de facto the potential barriers, then move away to reinitiate the passage of the next proton, and this, from close to close, by a kind of dynamic percolation. We have illustrated this mechanism in Fig. 4, D and E. It is relatively straightforward to estimate the gain in transfer probabilities of a proton with the same barrier height but having a modulated width. Thus, for example, a reduction of 1 A roughly increases the transfer probability by a factor of 10. Considering four barriers, the increase of the proton/electron transfer kinetics by the thermal fluctuations reaches almost half of two orders of magnitude. We thus provide here direct evidence that compressive RPV modes are involved in a charge transfer mechanism, carried out from site to site, and maintained by the action of localized vibrations. Detecting thermal hotspots allows to efficiently unveil which residues are potentially involved in reactive conformations, and from that the information of the structure. We have shown here that the H-cluster is in close interaction with most dynamically active residues of the protein structure. They all form a cavity surrounded by extensive compressive motions. This particular dynamic configuration, which involves the recruitment of almost half of the protein sequence of residues, illustrates what is believed to be necessary to achieve RPVs at the active site level. We also showed that this cavity was connected to a first group of residues located at thermal hotspots (C299 and S319) and themselves linked to a loop composed of three other residues (E279, E282, and R286). This network of five residues whose spacing is fairly regular (3.9 A) is demonstrated to couple with thermal fluctuations coming from the BB vibrations. Nevertheless, we notice that, at the level of the loop, E279, E282, and R286 form a fairly smooth stiffness gradient (Fig. 4 E), which decreases in rigidity as one approaches the solvent. We think that this structural property is a strategy commonly used by evolution to couple the dynamics of surface residues (close to a solvent), which is rather slow with the core of the protein (more rigid) subjected to faster fluctuations (43). The notion of a thermal hotspot also permits us to posit a conjecture regarding the temperature-dependence of catalytic kinetics, as quantified by Arrhenius and Eyring. Our observations reveal two potential effects. Below the classical limit (for temperatures below 200 K, limited to modes of 4 THz or less), modes localized within hotspots are subject to quantum mechanical freezing. The nonactivation of these modes may, in turn, hinder the RPV effect. Conversely, beyond the classical limit, the amplitude of vibrations becomes proportional to the square root of temperature (\sqrt{T}) , thus prompting a variation in the impact of compressing energy barriers.

On additional functional benefits of localized vibration

Wave localization effects are quite interesting from a functional point of view, as they allow employment of locally fast (picosecond) conformational rearrangements over lengthscales of ~ 1 A. These reorientations consist of compressions that occur not only between interchain residues but also between residues and water molecules (32). These compressions can also take the form of twisting and bending. In other words, localization effects provide the cavity with subtle reorganizations that can be coordinated in time and space. The local molecular movements that occur in concert within the enzyme structure are fully encoded in its folding. Hence, the thermal environment enables the exploration of a large number of atomic configurations, and the random but highly dense nature of residues' displacement fluctuations enhances the efficiency of finding configurations that favor charge transfers. In addition, once each of these transfers has been carried out, the high density of fast modes allows a prompt reset of the transfer networks to their "forward state". The characteristic timescale at which this occurs (picoseconds) is compatible with stabilization mechanisms. This is why we think that only QM/MM-MD calculations (32), jointly taking into account the thermal aspect associated with the dynamics of atoms at the complete topology of the BB chain (which is not at all the case for ab initio calculations) make it possible to predict barrier heights low enough to be compatible with the times of the chemical kinetics (31,32). This "thermal" activity that consists of a coupled chemistry with fold encoded thermal conformational fluctuations, appears here as an effective strategy to solve the problem of establishing a distinct transfer pathway for protons and electrons, while implying why the two phenomena occur in concert. The work of Artz et al. (12) has experimentally Please cite this article in press as: Chalopin et al., Phonon-assisted electron-proton transfer in [FeFe] hydrogenases: Topological role of clusters, Biophysical Journal (2023), https://doi.org/10.1016/j.bpj.2023.03.027

Chalopin et al.

shown the importance of specific reduction potentials associated with each Fe-S cluster. Indeed, the redox potential of each cluster has evolved to form a gradient from the solvent toward the active site, thus imposing a preferred direction for the electron flow. Indeed, if the modulation of the barriers by compression allows the formation of a specific transfer pathway, there is no chance that the corresponding fluctuations between amino acids impose any directionality in the electron flow. Thus, we suppose there was coevolution between these redox potentials (chemicals properties) and the fold-encoded pattern of localized modes (picosecond dynamical properties).

CONCLUSIONS

In this study, we have investigated the dynamic properties of [FeFe] hydrogenase, a key enzyme in the synthesis and consumption of molecular hydrogen. Our approach was based on a topological analysis of the protein's folded 3D structure, using the localization landscape to map the distribution of thermal motions within the system. By identifying hotspots of high phonon frequency density, we were able to show that the protein can be regarded as distinct islands of vibrational energy, with the FeS clusters forming a new topological network that dynamically couples these thermal hotspots. We found that the sets of residues involved in these hotspots corresponded to those reported previously as functionally important in the hydrogenase catalytic process. Our results suggest that Nature has solved the problem of enhancing chemical kinetics by using the energy of thermal fluctuations, localized according to the sequence, i.e., by selecting a specific chemistry/vibration coupling. Specifically, we have shown that this coupling operates through the intermediacy RPVs at the active site, and also the presence of the same type of localized vibration to ensure the coordinated transfer of electrons and protons. Our theory suggests that a biochemical function is not solely associated with the chemical nature of the active site residues, but also with the response of the structural and conformational environment to thermal agitation. Understanding the intricacy of these two phenomena open considerable avenues for the development of novel biomimetic catalysts.

SUPPORTING MATERIAL

Supporting material can be found online at https://doi.org/10.1016/j.bpj. 2023.03.027.

AUTHOR CONTRIBUTIONS

Y.C. developed the theory and performed the computations. S.P.C. and S.A encouraged Y.C. to investigate PETN in hydrogenase. S.A. managed the exchanges and the project from IFP énergies nouvelles. All authors discussed the results and contributed to the final manuscript.

ACKNOWLEDGMENTS

S.P.C. is supported by NIH GM-65440 and NSF MBP 2149122. Y.C. is supported by a public grant overseen by the French National Research Agency (ANR) as part of the "Investissements d'Avenir" program (Labex NanoSaclay, reference: ANR-10-LABX-0035). Y.C. would like to thank Dr. M. Buckle for fruitful discussions at the early stage of this work.

DECLARATION OF INTERESTS

The authors declare no competing interests.

REFERENCES

- Supran, G., S. Rahmstorf, and N. Oreskes. 2023. Assessing ExxonMobil's global warming projections. *Science*. 379:eabk0063. https://doi.org/10.1126/science.abk0063.
- Armstrong, F. A. 2004. Hydrogenases: active site puzzles and progress. Curr. Opin. Chem. Biol. 8:133–140. https://www.sciencedirect.com/ science/article/pii/S1367593104000195.
- Evans, D. J., and C. J. Pickett. 2003. Chemistry and the hydrogenases. Chem. Soc. Rev. 32:268–275.
- 4. Lubitz, W., H. Ogata, ..., E. Reijerse. 2014. Hydrogenases. *Chem. Rev.* 114:4081–4148. https://doi.org/10.1021/cr4005814.
- Duan, J., M. Senger, ..., M. Winkler. 2018. Crystallographic and spectroscopic assignment of the proton transfer pathway in FeFe -hydrogenases. *Nat. Commun.* 9:4726. https://doi.org/10.1038/s41467-018-07140-x.
- Karyakin, A. A., S. V. Morozov, ..., S. Cosnier. 2007. The limiting performance characteristics in bioelectrocatalysis of hydrogenase enzymes. *Angew. Chem. Int. Ed. Engl.* 46:7244–7246. https://doi.org/ 10.1002/anie.200701096.
- Peters, J. W., G. J. Schut, ..., M. W. W. Adams. 2015. FeFe and NiFe -hydrogenase diversity, mechanism, and maturation. *Biochim. Biophys. Acta*. 1853:1350–1369. https://www.sciencedirect.com/science/article/pii/S0167488914004194.
- Chenevier, P., L. Mugherli, ..., V. Artero. 2013. Hydrogenase enzymes: application in biofuel cells and inspiration for the design of noble-metal free catalysts for H2 oxidation. *Compt. Rendus Chem.* 16:491–505. https://www.sciencedirect.com/science/article/pii/S1631074812002895.
- Land, H., M. Senger, G. Berggren, and S. T. Stripp. 2020. Current state
 of [FeFe]-Hydrogenase research: biodiversity and spectroscopic investigations. ACS Catal. 10:7069–7086. https://doi.org/10.1021/acscatal.
 0c01614.
- Kleinhaus, J. T., F. Wittkamp, ..., U.-P. Apfel. 2021. [FeFe]-Hydrogenases: maturation and reactivity of enzymatic systems and overview of biomimetic models. *Chem. Soc. Rev.* 50:1668–1784. https://doi.org/10.1039/D0CS01089H.
- Birrell, J. A., P. Rodr'guez-Maciá, ..., W. Lubitz. 2021. The catalytic cycle of [FeFe] hydrogenase: a tale of two sites. *Coord. Chem. Rev.* 449:214191. https://www.sciencedirect.com/science/article/pii/S0010854521004653.
- Artz, J. H., D. W. Mulder, ..., J. W. Peters. 2017. Reduction potentials of [FeFe]-Hydrogenase accessory iron–sulfur clusters provide insights into the energetics of proton reduction catalysis. *J. Am. Chem. Soc.* 139:9544–9550. https://doi.org/10.1021/jacs.7b02099.
- 13. Pudney, C. R., A. Guerriero, ..., N. S. Scrutton. 2013. Fast protein motions are coupled to enzyme H-transfer reactions. *J. Am. Chem. Soc.* 135:2512–2517. https://doi.org/10.1021/ja311277k.
- Schramm, V. L., and S. D. Schwartz. 2018. Promoting vibrations and the function of enzymes. Emerging theoretical and experimental convergence. *Biochemistry*. 57:3299–3308. http://europepmc.org/ abstract/MED/29608286.
- Hay, S., and N. S. Scrutton. 2012. Good vibrations in enzyme-catalysed reactions. *Nat. Chem.* 4:161–168. https://doi.org/10.1038/nchem.1223.

- 16. Chalopin, Y., F. Piazza, ..., M. Filoche. 2019. Universality of fold-encoded localized vibrations in enzymes. Sci. Rep. 9:12835. https://doi. org/10.1038/s41598-019-48905-8.
- 17. Chalopin, Y. 2020. The physical origin of rate promoting vibrations in enzymes revealed by structural rigidity. Sci. Rep. 10:17465. https://doi. org/10.1038/s41598-020-74439-5.
- 18. Bruno, W. J., and W. Bialek. 1992. Vibrationally enhanced tunneling as a mechanism for enzymatic hydrogen transfer. Biophys. J. 63:689-699. https://www.sciencedirect.com/science/article/pii/S0006349592816545.
- 19. Klinman, J. P., and A. Kohen. 2013. Hydrogen tunneling links protein dynamics to enzyme catalysis. Annu. Rev. Biochem. 82:471-496. https://doi.org/10.1146/annurev-biochem-051710-133623.
- 20. Antoniou, D., M. R. Abolfath, and S. D. Schwartz. 2004. Transition path sampling study of classical rate-promoting vibrations. J. Chem. Phys. 121:6442–6447. https://doi.org/10.1063/1.1782813.
- 21. Chalopin, Y., and J. Sparfel. 2021. Energy bilocalization effect and the emergence of molecular functions in proteins. Front. Mol. Biosci. 8:736376
- 22. Quaytman, S. L., and S. D. Schwartz. 2007. Reaction coordinate of an enzymatic reaction revealed by transition path sampling. Proc. Natl. Acad. Sci. USA. 104:12253-12258. https://doi.org/10.1073/pnas. 0704304104.
- 23. Arcus, V. L., and C. R. Pudney. 2015. Change in heat capacity accurately predicts vibrational coupling in enzyme catalyzed reactions. FEBS Lett. 589:2200-2206. https://www.sciencedirect.com/science/ article/pii/S0014579315005797.
- 24. Hammes-Schiffer, S. 2015. Proton-coupled electron transfer: moving together and charging forward. J. Am. Chem. Soc. 137:8860-8871. https://doi.org/10.1021/jacs.5b04087.
- 25. Esselborn, J., N. Muraki, ..., T. Happe. 2016. A structural view of synthetic cofactor integration into [FeFe]-hydrogenases. Chem. Sci. 7:959–968. https://doi.org/10.1039/C5SC03397G.
- 26. Berggren, G., A. Adamska, ..., M. Fontecave. 2013. Biomimetic assembly and activation of FeFe -hydrogenases. Nature. 499:66-69. https://doi.org/10.1038/nature12239.
- 27. Wittkamp, F., M. Senger, ..., U. P. Apfel. 2018. FeFe -Hydrogenases: recent developments and future perspectives. Chem. Commun. 54:5934-5942. https://doi.org/10.1039/C8CC01275J.
- 28. Stripp, S. T., B. R. Duffus, ..., M. W. Ribbe. 2022. Second and outer coordination sphere effects in nitrogenase, hydrogenase, formate dehydrogenase, and CO dehydrogenase. Chem. Rev. 122:11900-11973. https://doi.org/10.1021/acs.chemrev.1c00914.
- 29. Land, H., A. Sekretareva, ..., G. Berggren. 2020. Characterization of a putative sensory [FeFe]-hydrogenase provides new insight into the role of the active site architecture. Chem. Sci. 11:12789–12801. https://doi. org/10.1039/D0SC03319G.
- 30. Mebs, S., M. Senger, ..., M. Haumann. 2017. Bridging hydride at reduced H-cluster species in [FeFe]-Hydrogenases revealed by infrared spectroscopy, isotope editing, and quantum chemistry. J. Am. Chem. Soc. 139:12157-12160. https://doi.org/10.1021/jacs.7b07548.

- 31. Lampret, O., J. Duan, ..., T. Happe. 2020. The roles of long-range proton-coupled electron transfer in the directionality and efficiency of FeFe -hydrogenases. Proc. Natl. Acad. Sci. USA. 117:20520-20529. https://doi.org/10.1073/pnas.2007090117.
- 32. Puthenkalathil, R. C., and B. Ensing. 2022. Fast proton transport in FeFe hydrogenase via a flexible channel and a proton hole mechanism. J. Phys. Chem. B. 126:403-411. https://doi.org/10.1021/acs. jpcb.1c08124.
- 33. Migliore, A., N. F. Polizzi, ..., D. N. Beratan. 2014. Biochemistry and theory of proton-coupled electron transfer. Chem. Rev. 114:3381–3465. https://doi.org/10.1021/cr4006654.
- 34. Leitner, D. M. 2008. Energy flow in proteins. Annu. Rev. Phys. Chem. 59:233–259. https://doi.org/10.1146/annurev.physchem.59. 032607.093606.
- 35. Gauquelin, C., C. Baffert, ..., I. Meynial-Salles. 2018. Roles of the F-domain in [FeFe] hydrogenase. Biochim. Biophys. Acta Bioenerg. 1859:69-77. https://www.sciencedirect.com/science/article/ pii/S0005272817301299.
- 36. Artz, J. H., O. A. Zadvornyy, ..., J. W. Peters. 2020. Tuning catalytic bias of hydrogen gas producing hydrogenases. J. Am. Chem. Soc. 142:1227-1235. http://europepmc.org/abstract/MED/31816235.
- 37. Sode, O., and G. A. Voth. 2014. Electron transfer activation of a second water channel for proton transport in [FeFe]-hydrogenase. J. Chem. Phys. 141:22D527. https://doi.org/10.1063/1.4902236.
- 38. Hong, G., A. J. Cornish, ..., R. Pachter. 2011. On understanding proton transfer to the biocatalytic [Fe-Fe]H sub-cluster in [Fe-Fe] H2ases: QM/MM MD simulations. Biochim. Biophys. Acta Bioenerg. 1807:510–517. https://www.sciencedirect.com/science/article/pii/S0005 272811000235.
- 39. Long, H., P. W. King, and C. H. Chang. 2014. Proton transport in Clostridium pasteurianum [FeFe] hydrogenase I: a computational study. J. Phys. Chem. B. 118:890-900. https://doi.org/10.1021/jp408621r.
- 40. Senger, M., V. Eichmann, ..., S. T. Stripp. 2019. How [FeFe]-Hydrogenase facilitates bidirectional proton transfer. J. Am. Chem. Soc. 141:17394-17403. https://doi.org/10.1021/jacs.9b09225.
- 41. Duan, J., A. Hemschemeier, ..., T. Happe. 2023. Cyanide binding to [FeFe]-Hydrogenase stabilizes the alternative configuration of the proton transfer pathway. Angew. Chem. Int. Ed. Engl. 62:e202216903. https://doi.org/10.1002/anie.202216903
- 42. Cornish, A. J., K. Gartner, ..., E. L. Hegg. 2011. Mechanism of proton transfer in FeFe -hydrogenase from Clostridium pasteurianum. J. Biol. Chem. 286:38341-38347. https://www.sciencedirect.com/science/ article/pii/S0021925820506777.
- 43. Zaragoza, J. P. T., A. Nguy, ..., J. P. Klinman. 2019. Detecting and characterizing the kinetic activation of thermal networks in proteins: thermal transfer from a distal, solvent-exposed loop to the active site in soybean lipoxygenase. J. Phys. Chem. B. 123:8662-8674. https:// doi.org/10.1021/acs.jpcb.9b07228.

Biophysical Journal, Volume 122

Supplemental information

Phonon-assisted electron-proton transfer in [FeFe] hydrogenases:

Topological role of clusters

Yann Chalopin, Stephen P. Cramer, and Simon Arragain

Supplementary Informations: Phonon-assisted electron-proton transfer in [FeFe] hydrogenases: Topological role of clusters

Yann Chalopin, Stephen P. Cramer, and Simon Arragain (Dated: February 27, 2023)

INTRODUCTION

MATERIALS AND METHOD

Construction of the dynamical matrix

To estimate harmonic interactions between residues, we implemented and compared two very distinct force elds, namely an elastic network model (ENM), as well as an all-atom force eld through molecular dynamics simulations. The elastic model employed here has no cut-o length. For the MD simulations, we employed the Amber force eld to take into account interactions between all the atoms of the enzyme. We have also simulated the interactions with the FeS cluster and H-cluster according to the force eld proposed by Kim. The solvent is accounted explicitly for the water atoms with the TIP3P potential, and by centering the system in a box such that the distance between an atom of the complex and the edge of the box is 10Å. The equilibrium trajectories of the system were obtained after minimizing the cohesion energy and an equilibration time of 0.1 ns in order to avoid too large conformational changes.

details

The constants α_{ij} of the system are obtained by tracking the equilibrium displacement—uctuations of the C_{α} . By introducing the correlation matrix \mathbf{C} of displacements

$$\mathbf{C}: (\mathbf{C})_{ij} = \beta < X_i X_j >, \tag{1}$$

with $\beta = 1/K_bT$. The force constant matrix A is obtained by inversion

$$\mathbf{A}: \alpha_{ij} = (\mathbf{C}^{-1})_{ij} \tag{2}$$

$$\mathbf{A}: \alpha_{ij} = \begin{cases} (\mathbf{C}^{-1})_{ij} & i \neq j \\ -\sum \alpha_{ij} & i = j \end{cases}$$
 (3)

However, the correlation matrix **C** contains noise which produces inaccurate matrix inversion by conventional methods. Instead it is decomposed in singular values as

$$\mathbf{C} = USV^T, \tag{4}$$

which allows to obtain the inverse matrix from

$$\mathbf{C}^{-1} = V S^{-1} U^T. \tag{5}$$

The correlation matrix was obtained and re ned by ensemble averaging 20 distinct equilibrated trajectories at room temperature (T = 300K). Figure 3-A(top) compares the location hotspots obtained from MD and ENM calculations. The correlation between the two quantities reaches 74%.

It can be seen that for a total of 574 residues, about 15 residues (< 3%) are thermal spots. As derived in a previous study, these domains populated with a high phonon density of states correspond to distinct, uncoupled clusters of residues (Figure 3-B). To further illustrate this assumption, we have projected this quantity onto the three-dimensional structure of the hydrogenase (Figure 3-C and Figure 3-D). The localization landscape reveals that the rigid, central region of the enzyme undergoes complex dynamic patterns, comprising small domains that form an irregular spatial structure. As discussed later, this distribution of thermal spots is crucial in the working of H_2 ases.

RESULTS

The topological role of the clusters

We provide an additional gure for this section

TUTORIAL: HOW TO COMPUTE THE LOCALIZATION LANDSCAPE

In this section, we will look at step by step how to calculate the localization landscape in detail. To do this, we will consider the simplest folded protein consisting of three residues. This simplicity allows us to present all the calculation steps that can be done by hand or analytically by the reader.

We start by expressing the dynamic matrix $L = -\Delta$ corresponding to the discrete Laplacian associated with the topology of the gure 5-B.

$$L = \begin{bmatrix} 1 & -1 & 0 & 0 \\ -1 & 3 & -1 & -1 \\ 0 & -1 & 2 & -1 \\ 0 & -1 & -1 & 2 \end{bmatrix}$$

This matrix can be seen as the sum of a degree matrix minus the adjacency matrix L = D - A. Now we express the matrix L_h obtained from Equation 1 describing the dynamics of the system in the harmonic regime de ned by the wave vector $k = \pi/a = \pi$. So:

$$Lh = c - \Delta_h \begin{bmatrix} c - 1 & 1 & 0 & 0\\ 1 & c - 3 & 1 & -1\\ 0 & 1 & c - 2 & 1\\ 0 & -1 & 1 & c - 2 \end{bmatrix}$$

We choose c to be greater than the largest eigenvalue of the system (here we choose for example c = 6).

$$Lh = c - \Delta_h \begin{bmatrix} 5 & 1 & 0 & 0 \\ 1 & 3 & 1 & -1 \\ 0 & 1 & 4 & 1 \\ 0 & -1 & 1 & 4 \end{bmatrix}$$

The solution of the linear system de ned by Equation (3)

$$L_h u_h = (1) (6)$$

gives us $u_h = [0.125, 0.375, 0.075, 0.325]$. This localization landscape is plotted on Figure 5-C and represented in space on Figure 5-D with an identical color code to the one representing the results of the article. In the rst case (C), the landscape is plotted as a function of the residue index encountered in the PDB in order to avoid discontinuity in the case where the sequence contains gaps.

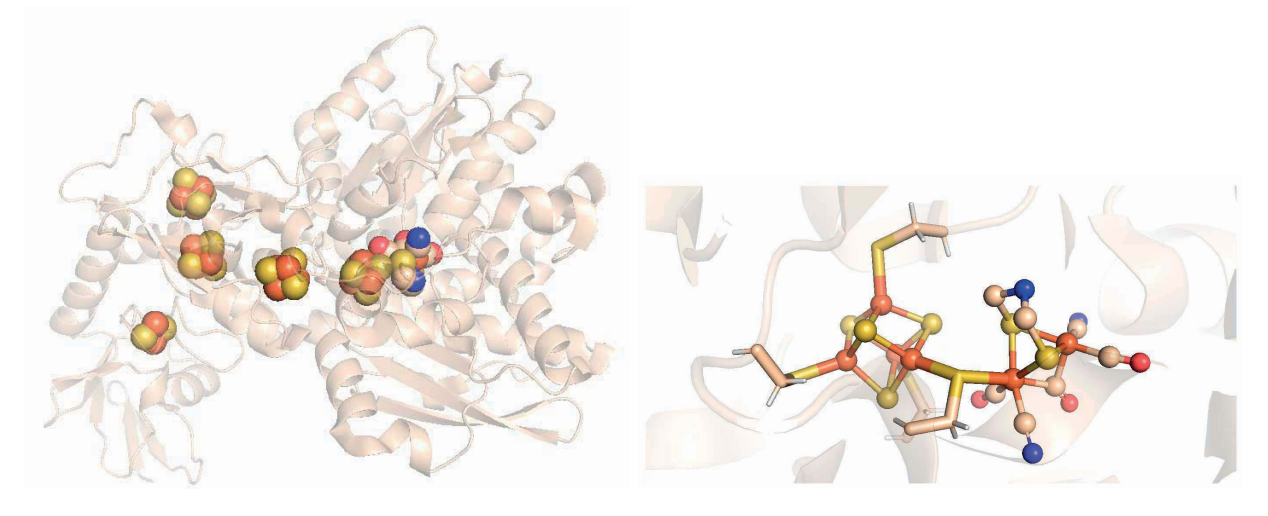


FIG. 1: **Structure** [FeFe] hydrogenase (CpI) with all the FeS clusters and the details of the H-Cluster with carbon in orange, oxygen in red, sulfur in yellow, nitrogen in blue et iron deep red (PDBid: 4xdc).

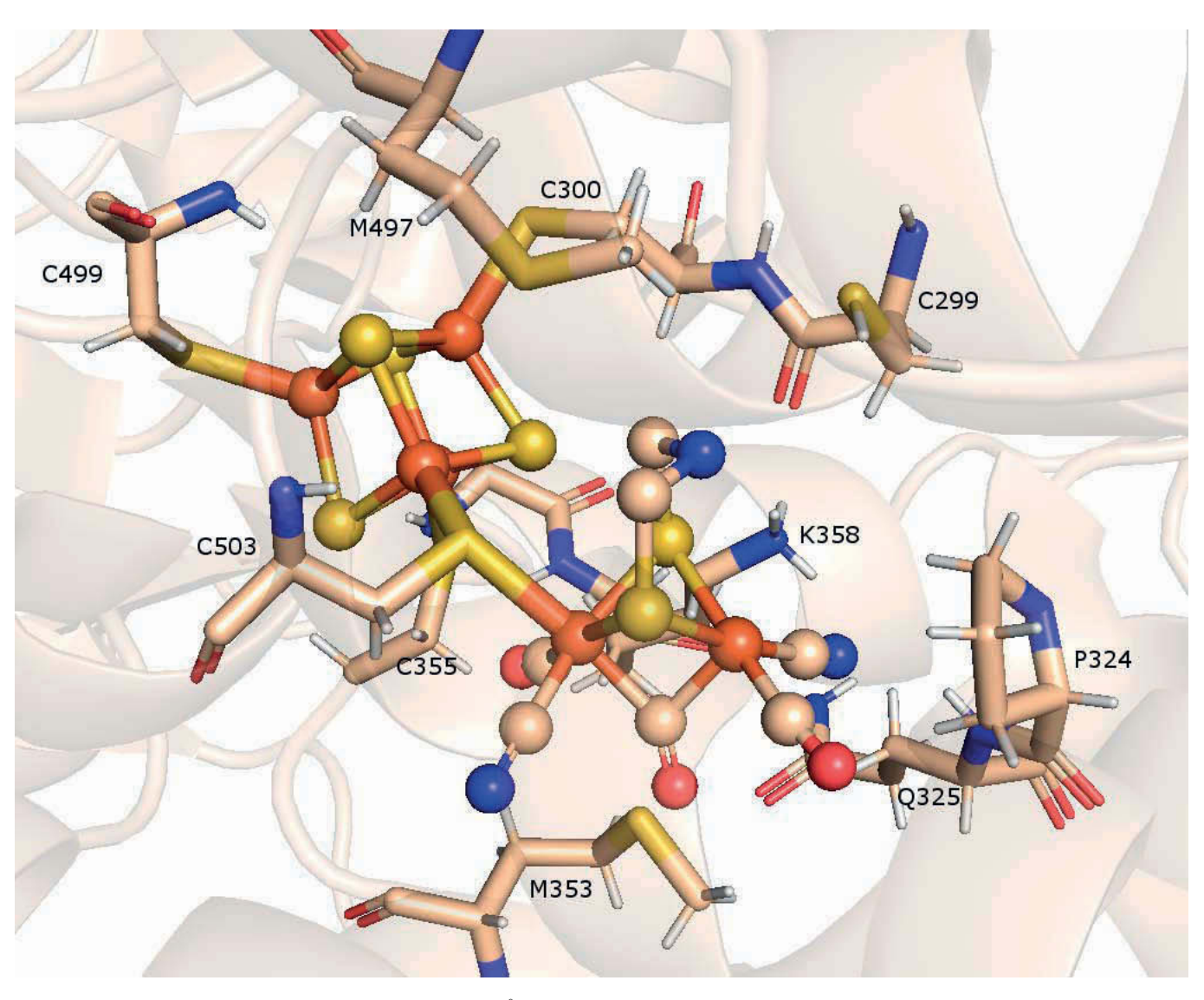


FIG. 2: **Structure** CpI amino acid arround 4Å of the subcluster of the H-Cluster (Top part). The amino acids inCpI M353, C299, C298, M497, K358,P324, Q325. CpI additional residues arround the subcluster might also be important (S323, I268, A230, P231, S232, P354,F417,

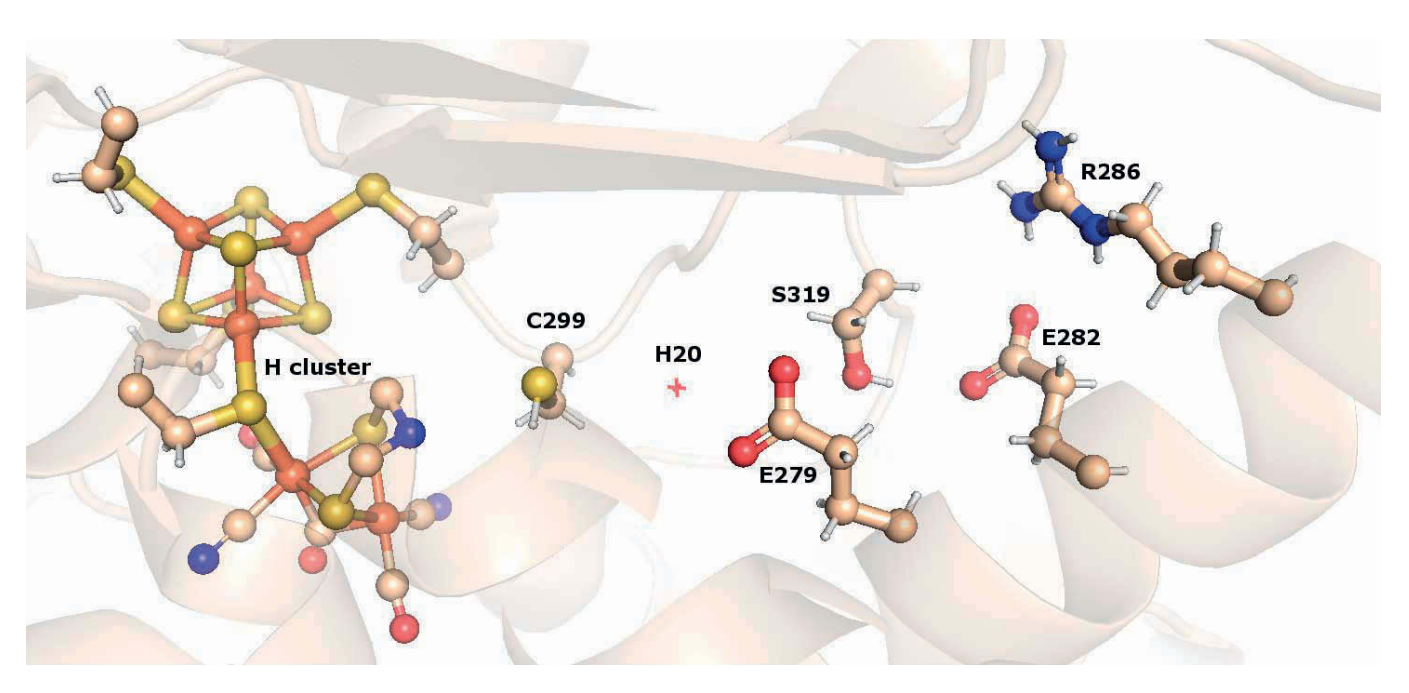


FIG. 3: Structure Proton transport chains in CpI with in the pathway 2, C299, S298, some H_2O molecules [Ginovska-Pangovska 2014].

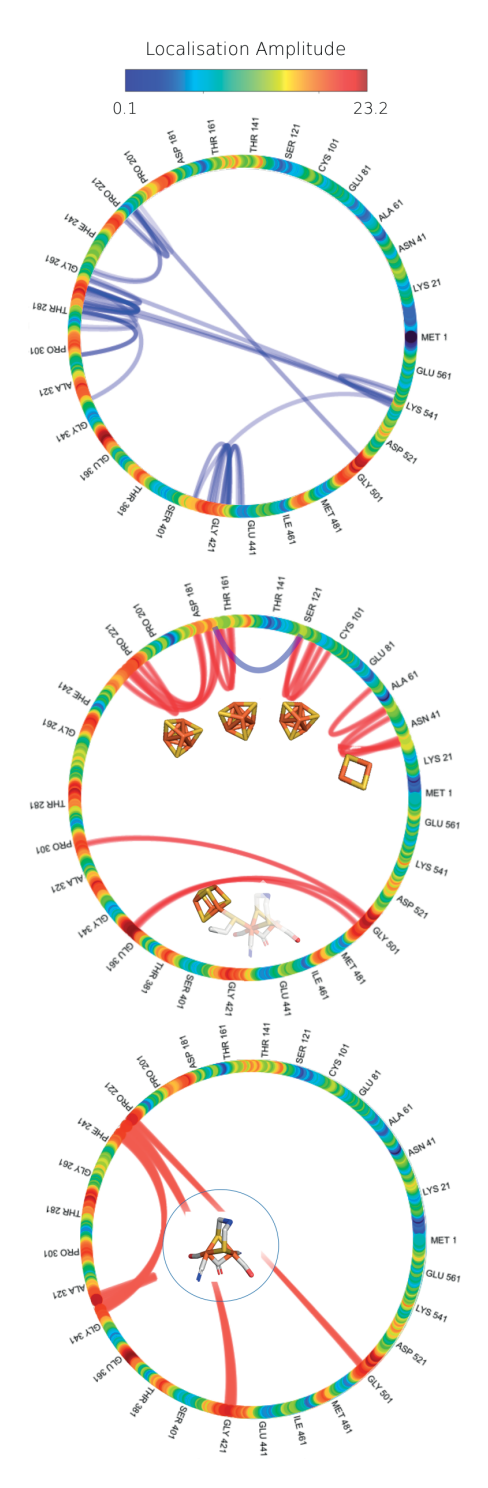


FIG. 4: Thermal hot spots and distal contacts top: Main interactions between non consecutive residues in the sequence. This indicates that speci-c hot-spots are dynamically coupled by distal contacts. middle: The FeS clusters allows to couple most of the thermal hot-spots of the structure. They play the role of cofactor-contacts. bottom: The H-cluster is at the center of a cavity made of hot-spot. The pocket is associated to network of connected residues that are the main hot-spots. Units are in ω^{-2}

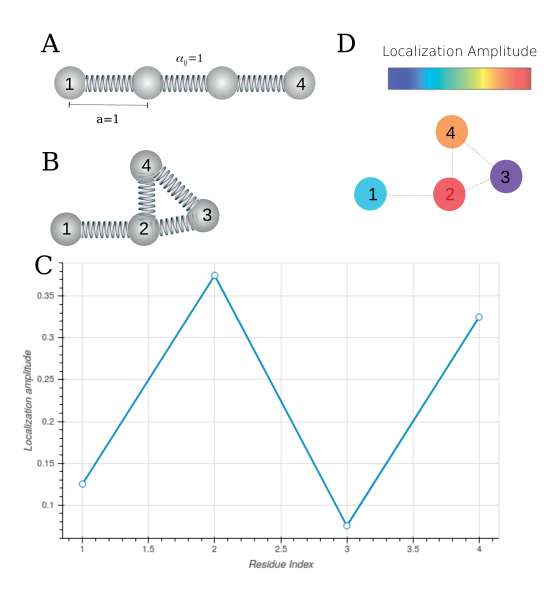


FIG. 5: Computing the localization landscape top:
A - Simple homogeneous non folded model of protein.
B. Simple folding of a 4 residues protein.
Corresponding localization lanscape.
D. Color coded spatial representation of the localization landscape.